

21 cm Absorption Studies with the Square Kilometer Array

N. Kanekar^a, F. H. Briggs^b

^aKapteyn Institute, University of Groningen, The Netherlands

^bRSAA, The Australian National University, Mount Stromlo Observatory, Australia

^bAustralia Telescope National Facility, Sydney, Australia

HI 21 cm absorption spectroscopy provides an excellent probe of the neutral gas content of absorbing galaxies, yielding information on their kinematics, mass, physical size and ISM conditions. The high sensitivity, unrivaled frequency coverage and RFI suppression techniques of the SKA will enable it to use HI absorption to study the ISM of high column density intervening systems along thousands of lines of sight out to high redshifts. Blind SKA 21 cm surveys will yield large, unbiased absorber samples, tracing the evolution of normal galaxies and active galactic nuclei from $z \gtrsim 6$ to the present epoch. It will thus be possible to directly measure the physical size and mass of typical galaxies as a function of redshift and, hence, to test hierarchical models of structure formation.

1. INTRODUCTION

The epoch at which objects of a particular mass scale form is a critical test of cosmological models. Theoretically favored structure formation scenarios¹ predict that large galaxies are formed in hierarchical fashion, with smaller cold dark matter (CDM) halos merging to form larger ones, followed by the dissipative re-collapse of baryons into the resulting deep gravitational potentials (e.g. [61]). Such CDM-based hierarchical merger models have the generic feature that big galaxies are formed at late times ($z \lesssim 1$), in order to remain consistent with the observed anisotropies in the microwave background. The period between redshifts $z \approx 5$ and $z \approx 1$ is thus expected to be one of vigorous assembly of galaxies.

Measuring the typical size and mass of galaxies as a function of redshift allows us to directly test the hierarchical merger paradigm. Unfortunately, this has been difficult to carry out in practice. While both the number density of luminous quasars and the star formation rate (SFR) density in Lyman-break galaxies appear to peak at $z \approx 2$ (e.g. [40,55,56]), these observations are strongly biased toward the bright end of the luminosity

function and may not probe the behavior in “typical” systems. Further, the stellar mass detected in Lyman-break galaxies at these redshifts is but a fraction of the neutral gas mass in all galaxies, implying that the observations are not sensitive to the bulk of the baryons.

One of the SKA goals is the direct monitoring of the HI content of collapsed objects, from the epoch of formation right through to the present day (see contribution by van der Hulst et al., this Volume). In fact, the square kilometer of aperture is a consequence of the interest in mapping gas-rich galaxies out to redshifts as high as $z \sim 1$. This stems from a natural desire to image the high- z galaxies in the same fashion as done by the VLA and WSRT for systems at $z < 0.05$. Alas, the frontier of galaxy evolution studies has moved to higher redshifts, where even the SKA will have trouble detecting massive galaxies and will not make maps with significant structural and kinematic information.

HI 21 cm absorption measurements toward radio-loud background sources (either quasars or radio galaxies) can provide interesting information on the structure and physical conditions in high redshift galaxies (e.g. [32] and references therein). To date, a number of technical factors (e.g. frequency coverage, spectrometer bandwidth/resolution, RFI environment, ade-

¹Including the currently standard Λ -CDM “concordance cosmology”, with $\Omega_m = 0.27$, $\Omega_\Lambda = 0.73$, $H_0 = 71 \text{ km s}^{-1} \text{ Mpc}^{-1}$; this model will be used for numerical estimates in the current article.

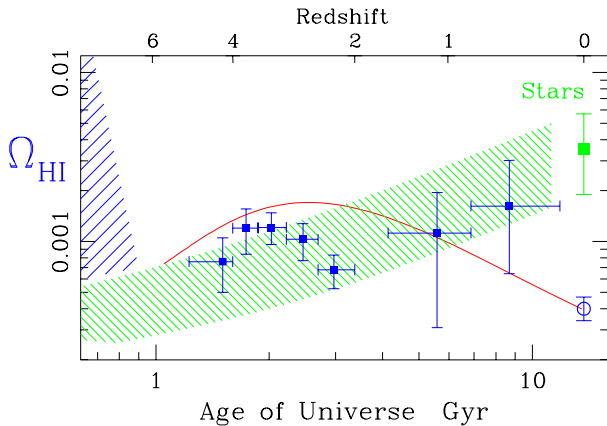


Figure 1. Neutral gas content of the Universe as a function of time, expressed as a fraction of the critical density at the present epoch. The filled squares for $5 > z > 2$ are from “blind” optical DLA surveys [50], the filled squares for $1.6 > z > 0$, from MgII-selected DLA surveys [42] and the open circle at $z = 0$, from HI emission surveys [72]. The light shaded region indicates the rising trend of stellar mass with time, leading to the filled square for the present stellar mass in galaxies [25]. The solid curve for the evolution of HI density with time indicates the spirit of the dust-corrected models of [44]. The darker shading to the left at $z > 6$ reflects the rise in baryon neutral fraction during the Epoch of Reionization [2,22].

quate collecting area, etc) have combined to hinder such studies with current radio telescopes. We describe in this chapter the potential of the SKA to improve our understanding of galaxy evolution through absorption studies in the HI 21 cm line.

2. DAMPED LYMAN- α SYSTEMS

Absorption line studies toward bright background sources provide a powerful observational probe of galaxy formation and evolution. While emission studies of a flux-limited, high redshift sample are usually dominated by the brightest (often atypical) sources, absorption samples

are likely to be more representative of “normal” galaxies at a given redshift, since the most common objects that host HI clouds will provide the largest cross section for chance intervention toward high z radio sources. The high HI column density absorbers, the damped Lyman- α systems (DLAs, with $N_{\text{HI}} \gtrsim 10^{20} \text{ cm}^{-2}$) are of particular interest as these are the largest repository of neutral gas at high redshifts and hence believed to be the precursors of present-day galaxies (e.g. [67]). As indicated in Figure 1, the HI mass density in DLAs at $z \sim 3$ is a factor ~ 4 larger than that observed today, but comparable to the stellar mass density in luminous galaxies at $z \sim 0$ (e.g. [57]). This is consistent with a picture of gas depletion with time due to star formation, exchanging the neutral gas density for mass locked in populations of long-lived stars.

Understanding the evolution of a “typical” DLA with redshift is critical to understanding normal galaxy evolution. Specifically, one might directly test structure formation models by measuring the typical sizes, structures and dynamical masses of an unbiased sample of DLAs as a function of redshift. Such a sample could also be used to understand the evolution of physical conditions in the interstellar medium of normal galaxies, the onset of star formation, etc.

Despite twenty five years of detailed study, the typical nature of high z DLAs remains a controversial issue, with models ranging from large, rapidly rotating massive disks (e.g. [48]) to small, merging sub-galactic systems (e.g. [27]). Similarly, physical conditions in the ISM of the absorbers are also the subject of much debate, with some authors claiming evidence that most of the HI is in a cold phase [68] and others arguing for predominantly warm gas [32,45]. Studies of DLA chemical abundances have also found only weak evidence for evolution [46,49], with low metallicities ($[\text{Zn}/\text{H}] \lesssim -1$) typical even at low redshifts. This is somewhat surprising if the absorber population evolves into the population of large galaxies of solar metal abundance that dominate the absorption cross-section in the Universe today [51,70,71].

There are a number of reasons for the general contention surrounding the nature of damped ab-

sorbers. Present DLA samples contain two obvious biases, which complicates their use in studying the evolution of the average galaxy population. First, it has only been possible to carry out extensive spectroscopic surveys for DLAs at redshifts $z_{\text{abs}} \gtrsim 1.7$, as it is here that the Lyman- α line is observable with ground-based telescopes; current DLA samples are hence strongly biased toward high redshifts, presenting a snapshot of the Universe during the time window at 10 – 30% of its present age. The redshift range $0 < z \lesssim 1.7$ comprises 70% of the age of the Universe, covering the stages where proto-galactic systems evolve to present-day galaxies in hierarchical merger scenarios. Further, the high z DLA samples are almost entirely drawn from optically selected surveys (e.g. [67,57]; but see [20]) and may be biased against systems with a high metallicity (i.e. a high dust content; see, for example, [21]). Piecing together the puzzle critically requires an unbiased sample of DLAs with a uniform sampling in redshift; as will be seen later, this can be achieved through absorption surveys in the HI 21 cm line.

In addition to current biases, it has so far proved very difficult to distinguish between different models by direct observations of DLAs at high redshift. Direct imaging is restricted by large observing time requirements at all wavebands; optical imaging studies are further complicated due to problems with subtracting out the point spread function of the background QSO. Similarly, it is not possible to determine the transverse size of the absorbers using optical or ultraviolet absorption lines as the background AGN source is unresolved at these wavelengths; even cases of multiply lensed images provide very few lines of sight through the intervening galaxy. Radio absorption studies provide perhaps the only hope in this regard as it is only in this waveband that some sources have extended background continuum sources, against which one might determine the transverse size and kinematics of the absorbing galaxy. Of course, the vast quantities of neutral hydrogen at high redshifts make the HI 21 cm line the obvious transition for this purpose.

3. 21 CM ABSORPTION STUDIES

The HI column density N_{HI} of a homogeneous cloud in thermal equilibrium is related to its 21 cm optical depth τ_ν and spin temperature T_s by the expression

$$N_{\text{HI}} = 1.823 \times 10^{18} T_s \int \tau_\nu dV , \quad (1)$$

where N_{HI} is in cm^{-2} , T_s in K and dV in km s^{-1} . In the optically thin limit, this expression relates N_{HI} to the emission brightness temperature T_B as $N_{\text{HI}} = 1.823 \times 10^{18} \int T_B(V) dV$. When optical depth is computed from the ratio of flux density in the absorption line depth ΔS_ν to the integrated source continuum S_ν , the assumption is often made that a layer of uniform spin temperature and HI column density covers a fraction f of the background source, leading to $\tau_\nu = -\ln(1 - \Delta S_\nu / f S_\nu)$

The relatively weak strength of the 21 cm transition implies that 21 cm absorption is only detectable in high column density gas. This can be clearly seen from Equation (1); typical 21 cm equivalent widths² are $W_V \sim 1 \text{ km s}^{-1}$ while spin temperatures are usually $\gtrsim 100 \text{ K}$. These parameters lead to typical HI column densities $N_{\text{HI}} \gtrsim 10^{20} \text{ cm}^{-2}$, precisely those that would give rise to damping wings in the Lyman- α line. 21 cm absorption surveys are thus well-matched toward the construction of DLA samples. Further, such surveys contain no “intrinsic” redshift bias, such as that arising from the ultraviolet cut-off in the atmosphere. And, of course, flux-limited radio samples are unaffected by dust. Blind surveys in the 21 cm line could be used to obtain DLA samples unbiased by dust extinction and redshift coverage. On the other hand, the spin temperature dependence inflicts a bias toward cold gas on blind surveys, and the allocation of radio frequency bands to communications and navigation services excludes those bands from blind surveys for observatories located in industrialized regions of the world.

²Note that the equivalent width is defined here as $W_V \equiv \int \tau dV$ (e.g. [32]), unlike the usual definition $W_\lambda \equiv \int (1 - e^{-\tau_\lambda}) d\lambda$, used when $\tau_\lambda \gtrsim 1$

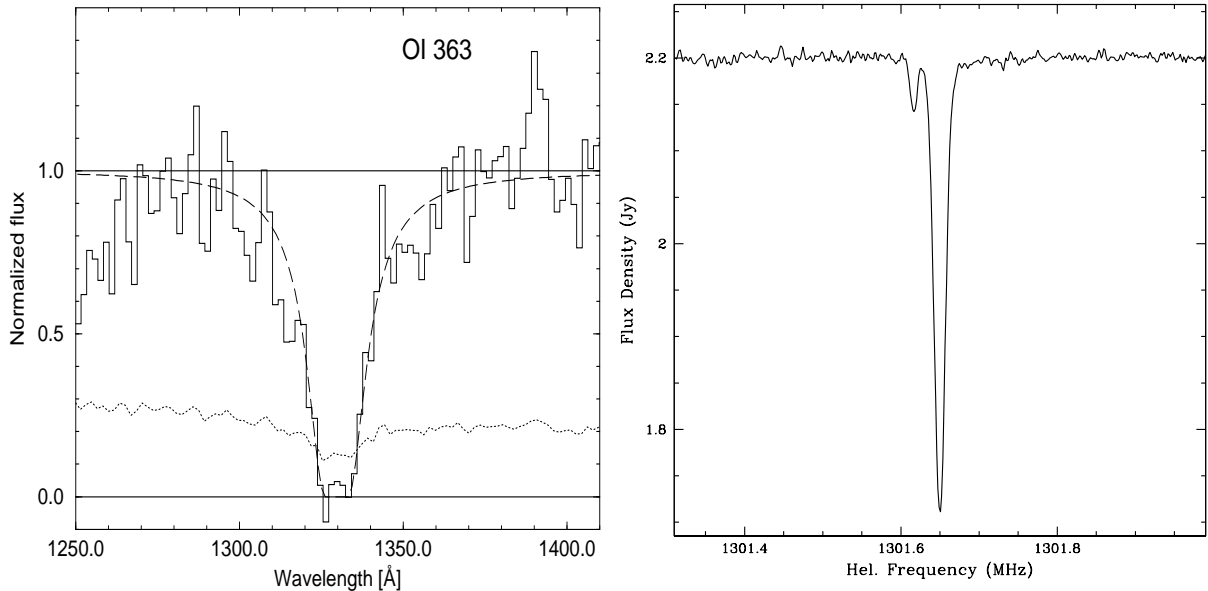


Figure 2. [A] Left panel : The $z = 0.0912$ damped Lyman- α line toward QSO 0738+313, obtained with HST-FOS [52]. [B] Right panel : The 21 cm profile of the above absorber, obtained with Arecibo [38].

Figure 2 shows a comparison between the damped Lyman- α and 21 cm spectra for the $z \sim 0.0912$ DLA toward QSO 0738+313 [52,38]. The Lyman- α line is highly saturated, allowing the DLA line to provide no kinematic information on the absorbing galaxy; the less saturated metal lines in these systems are often diagnostics of complex kinematic structure [48]. Unlike the 21cm absorption, the DLA line is insensitive to the temperature of the absorbing gas. While the 21 cm absorption in this $z \sim 0.0912$ absorber is stronger than usual in redshifted systems, the peak optical depth is still only ~ 0.24 , implying that the profile might be used to glean information on the kinematics of the absorber. In fact, the 21 cm absorption profile in this absorption against QSO 0738+313 could be decomposed into three components, two arising from absorption in cold (~ 100 K) gas and the third in the warm phase, at a kinetic temperature of ~ 5500 K [38]. Thus, while the damped Lyman- α line di-

rectly provides the HI column density along the line of sight, 21 cm studies are extremely useful in detailed studies of both kinematics and physical conditions of gas in galaxies.

4. HI KINEMATICS : SPATIAL MAPPING OF 21 CM ABSORPTION

The goals of mapping the gas components of galaxies at high redshift are: (1) determine the physical sizes of the galaxies, (2) measure the kinematics of the system, (3) assess whether the system is disk-like or a recent, turbulent remnant of formation, and (4) if disk-like, compute the effective dynamical mass for use in testing theories for the assembly of galaxies. The most direct way of doing this is through 21 cm *emission* observations; unfortunately, the sensitivity of current-day radio telescopes limits such studies to local objects. In fact, we will see in Section 7 that prohibitively large amounts of time would be needed even with the SKA to image large samples of high

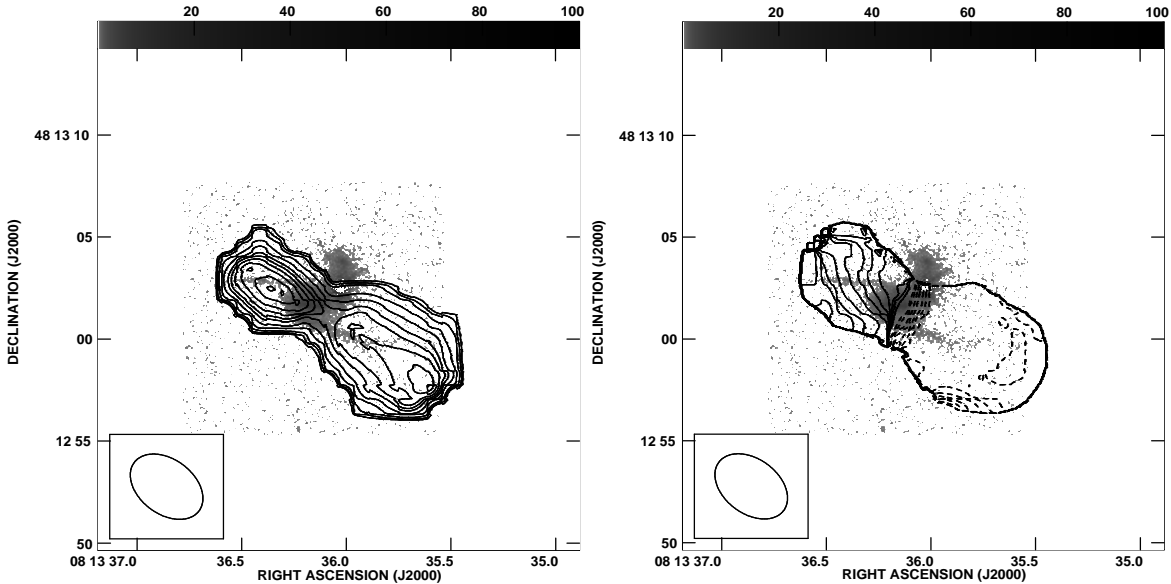


Figure 3. [A] Left panel : The integrated 21 cm optical depth toward 3C196 (contours; [35]), overlaid on an HST image (greyscale; [54]). [B] Right panel : The integrated 21 cm absorption velocity field toward 3C196 (contours; [35]), overlaid on an HST image (greyscale; [54]).

z galaxies in the 21 cm line.

Constraints on the size and gas kinematics of DLAs can also be obtained from high angular resolution 21 cm *absorption* studies, provided the background radio continuum is extended on scales larger than the telescope resolution element [35]. Of course, there are differences between kinematic studies in absorption and in emission. Spatially resolved emission studies directly provide the HI mass of the galaxy³, its physical extent, velocity field and dark matter potential. On the other hand, less information is available in absorption since the observations are only sensitive to the kinematics of gas lying in front of the background radio continuum (e.g. [10]). Further, mapping the absorption does not measure the HI mass directly but only the optical depth; one must assume a spin temperature to obtain an estimate of the HI mass of the absorber⁴. Absorption and emission studies are also sensitive to slightly dif-

ferent velocity fields, weighted by optical depth against the structure in the background continuum source in the former case and by column density in the latter. Both provide information on whether the velocity field is quiescent (i.e. well-ordered) or whether disruptive events (e.g. mergers) have occurred in the recent past. Given sufficient spatial resolution and sensitivity, it is possible to model the absorption velocity field to obtain the dynamical mass. In fact, even in the absence of high spatial resolution 21 cm line observations, spectral modeling in combination with knowledge of the background radio structure can constrain properties of the absorbing galaxy [12,33]. Finally, absorption mapping provides a lower limit to the physical extent of the galaxy. The full application of absorption studies will generally require statistical analysis of a large number of systems.

Spatial mapping of 21 cm absorption requires the identification of DLAs toward extended radio sources such as radio galaxies. The median size of

³Assuming that the emission is optically thin.

⁴ $T_s \sim 100$ K provides a fairly good lower limit to the mass.

high z radio galaxies (~ 50 kpc) is well matched toward testing whether large gaseous disks are common at high redshift. Radio galaxies usually have weak optical counterparts, implying that it is difficult to find such systems through optical spectroscopic surveys, since the latter target optically bright QSOs, which tend to have compact radio structure. On the other hand, surveys selecting DLA absorbers through 21 cm absorption toward radio galaxies would also provide interesting objects for follow-up optical imaging. PSF subtraction should not be an issue here as there would be little bright optical continuum; this would aid the optical identification of the intervening galaxy.

A number of VLBI 21 cm observations have studied absorption against compact radio components of the background QSO, at high spatial resolution (e.g. [63,38,7]). However, at present, the paucity of absorbers toward radio galaxies and poor frequency coverage of radio interferometers has meant that mapping studies sensitive to galactic disk scales of ~ 10 kpc have only been possible in two DLAs, at $z \sim 0.4$. Figs. 3[A] and [B] show the zeroth and first velocity moment of the integrated 21 cm absorption toward 3C196, obtained with the GMRT [35]. The two main components of the 21 cm profile were found to arise from absorption in two arms of a large barred spiral, against the south-west hotspot and the eastern lobe of 3C196, as had been deduced by [12]. HI absorption was detected out to a radius of ~ 70 kpc, far beyond the extent of the optical galaxy. The authors have also resolved the 21 cm absorption from the $z \sim 0.395$ DLA toward PKS 1229–021, showing that the absorber has a physical size larger than ~ 30 kpc, again a result that had been earlier inferred from modeling the unresolved 21 cm spectrum obtained at the WSRT [9].

It should be pointed out that current telescopes are very unlikely to make significant advances in mapping 21 cm absorption at redshifts higher than $z_{\text{abs}} \sim 0.5$. Sensitive interferometers such as the GMRT and the VLA do not have sufficiently long baselines to map the absorption; for example, the GMRT has a spatial resolution of ~ 25 kpc at 610 MHz, i.e. at $z_{\text{abs}} \sim 1.3$. At

the other extreme, very long baseline interferometers like the VLBA resolve out most of the extended background emission, due to the absence of short baselines. Progress in this field requires interferometers with wideband frequency coverage and modest angular resolution ($0.1''$) to resolve $\lesssim 1$ kpc at $z \sim 1 - 5$ (corresponding to baseline lengths $B \gtrsim 600(1+z)$ km). Mapping of complex sources would also require good U-V coverage and a high sensitivity. The large antennas of the EVN+Merlin would be a good match to this problem in the near term but for the high level of background radio communication signals throughout Europe, which lessen the feasibility for equipping the arrays with appropriate receivers. Some progress in mapping absorption against background sources of simple structure might be made through continuum mapping in standard radio astronomy bands that bracket the absorption frequency, followed by line observations with a few well chosen baselines and model fitting to tie the HI absorption features to specific lines of sight.

5. ISM CONDITIONS : THE SPIN TEMPERATURE

If the HI column density toward a radio-loud QSO can be obtained from independent observations (e.g. from the damped Lyman- α profile, soft X-ray absorption, etc), a measurement of the 21 cm optical depth can be used in equation (1) to estimate the spin temperature. In contrast to mapping studies, these experiments are most easily accomplished with compact background sources, so that the line of sight toward the optical or ultraviolet source is the same as that toward the radio continuum. For more complex sources, VLBI mapping is necessary to isolate only those 21cm absorbing clouds that contribute to absorption against the QSO nucleus.

In the Galactic interstellar medium, the spin temperature T_s of cold, dense HI clouds (comprising the “cold neutral medium”; CNM) is simply the kinetic temperature T_k of the cloud [23,36]; on the other hand, $T_s \leq T_k$ for the lower density, “warm neutral medium” (WNM) [39]. For multi-phase structure along a line of sight, the net T_s is

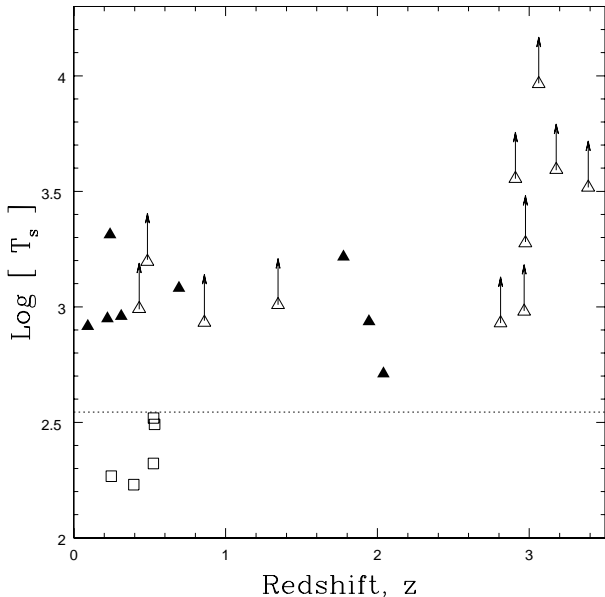


Figure 4. The spin temperature ($\text{Log}[T_s]$) as a function of redshift for the 24 DLAs of the present sample [32]. Objects identified with spiral galaxies are plotted using squares; other detections are shown as filled triangles, with non-detections shown as open triangles, with arrows.

the column-density-weighted harmonic mean of the temperatures of different phases (e.g. [36]), and T_s is biased toward the cold gas. For example, assuming typical temperatures of ~ 100 K and ~ 8000 K for the cold and warm phases, a line of sight with half the gas in each phase would have $T_s \sim 200$ K, while one with 90% of the gas in the WNM and only 10% in the CNM would have $T_s \sim 900$ K. The spin temperature thus provides information on the fraction of neutral gas at different temperatures, that might be used to study the evolution of the ISM with redshift.

Even more interesting, however, T_s may serve as an indicator of galaxy type. This is because the global fractions of cold and warm neutral gas in a galaxy are likely to be primarily determined by its central pressure and average metallicity [69].

Large spiral galaxies like the Milky Way are expected to have relatively large amounts of CNM, as such systems have both a high central pressure (due to their large mass) and a high metallicity; the Milky Way has roughly equal amounts of warm and cold HI. On the other hand, the low metallicities and pressures in smaller systems like dwarf galaxies are not conducive to the formation of the cold phase. This occurs because the ISM in small galaxies cools inefficiently, due to the lack of metals (and hence a lack of radiation pathways); such systems are hence expected to have a substantially higher HI fraction in the warm phase. An average line of sight through a mature large spiral should thus have a systematically lower spin temperature than an average line of sight through a low-metallicity, dwarf galaxy.

Typical lines of sight in the Milky Way and local spirals like Andromeda have $T_s \lesssim 200$ K (e.g. [3]). In contrast, two decades of observations have found that the majority of DLAs have significantly higher spin temperatures, $T_s \gtrsim 700$ K (e.g. [64,65,66,59,14,8,37,15,17,31,32]). Figure 4 shows a plot of the measured spin temperatures as a function of redshift for the 24 DLAs of the present 21 cm absorption sample [32]. Both low and high T_s values are found at low redshift $z < 1$, while all high redshift ($z \gtrsim 3$) DLAs have high T_s . Present results thus suggest that high z DLAs have fairly small CNM fractions, with most of the gas in the warm phase. Figure 4 also hints at evolution in the relative fraction of the cold and warm phases from high redshifts to today.

The key to understanding the evolution in T_s is the anti-correlation found between T_s and metallicity $[\text{Zn}/\text{H}]$ in a sample of 15 DLAs drawn from all redshifts [34]; this finding implicates gas metallicity in determining the temperature of the neutral ISM. At high redshift, there is a larger fraction of primitive, low-enrichment ISM gas in the cross section provided by the random intervening clouds.

In the low redshift range of the sample plotted in Figure 4, all five low z , low T_s DLAs have been identified with luminous spiral galaxies [13,53]. In contrast, the low z DLAs with $T_s \gtrsim 700$ K have been found to be associated with dwarf or low surface brightness (LSB) systems (e.g. [53,

18]). The current low z sample thus suggests that T_s can indeed “distinguish” between intervening dwarfs and large spirals for galaxies in the nearby universe. This correlation relies on the primitive nature of the dwarf irregular and LSB galaxies so that their level of metal enrichment lies below that of the more evolved large spirals, and hence their cooling is less efficient, and their observed spin temperature is higher.

While it may be tempting to argue that high redshift absorbers with high spin temperatures are small galaxies, the only clear physical evidence on their nature is that their ISM gas is primitive material of low-metallicity. Determination of physical sizes and masses of the absorbers awaits measurement by the next generation of radio telescopes.

6. ASSOCIATED 21 CM ABSORBERS

Blind 21 cm surveys will also yield large samples of *associated* absorption systems, probes of the local environments of radio galaxies and quasars (e.g. [26,19,41,60,47]). This will allow detailed studies of the kinematics and distribution of gas close to the AGN, important for understanding the physics of AGN activity, especially since this activity may well be fueled (and perhaps even triggered) by the neutral gas (e.g. [26]). Such observations allow direct tests of the unification scheme for radio galaxies and quasars (e.g. [1]). For example, such schemes predict that the line of sight to broad line radio galaxies is normal to the torus (and the thick disk), while that toward narrow line radio galaxies lies close to the plane of the torus. Associated 21cm absorption should thus be systematically more common in the latter class of systems as the nucleus in broad line systems is not expected to be obscured by the neutral gas. Preliminary evidence for this effect has already been found (e.g. [41]), but the number of systems in the sample is quite small and restricted to fairly low redshifts ($z \lesssim 0.2$). Similarly, van Gorkom et al. [26] find a clear preponderance of infall in local radio galaxies while Vermeulen et al. [60] show tantalizing evidence that outflows are more common than infall at intermediate redshifts ($0.2 \lesssim z \lesssim 0.8$). While the

two results hint at evolution in the nuclear environment, small number statistics again make it difficult to draw firm conclusions. The SKA 21 cm surveys (see also the contribution of Jarvis & Rawlings, this Volume) will provide homogeneous samples of associated absorbers out to at least $z \sim 6$, allowing us to trace in detail any evolution in nuclear environments (e.g. disk size, the existence of outflows and infall, etc) from high redshifts to the present epoch.

7. PROSPECTS WITH THE SKA

An important step to using DLAs as tracers of galaxy evolution is setting up an unbiased absorber sample; this can be done through blind 21 cm absorption surveys toward radio-loud sources. The weakness of the 21 cm transition implies that high sensitivity is needed for such surveys, especially since they must perforce be carried out at fairly high spectral resolution (21 cm lines can be fairly narrow, with FWHM $\gtrsim 5 \text{ km s}^{-1}$; e.g. [16]). Further, for a cosmologically distant absorber, the 21 cm line redshifts out of the “protected” 1420 MHz radio band into frequency ranges allocated to communication and navigation services; carrying out astrophysical observations at such frequencies is a serious challenge. Of course, wideband frequency coverage is a pre-requisite to carrying out the survey observations. And, finally, mapping absorbers from the resulting sample requires moderately high spatial resolution and benefits from good U-V coverage.

Sensitivity, frequency coverage, RFI and angular resolution have long been the rocks on which radio telescopes have foundered in their attempts to use 21 cm absorption studies as a probe of structure formation in the Universe. All of these issues will be addressed in the SKA and are briefly discussed below; the specifications are from [30].

1. Sensitivity : The specifications for the SKA sensitivity at low frequencies are $A_{eff}/T_{sys} = 5000$ at 200 MHz and $A_{eff}/T_{sys} = 20000$ between 0.5 and 5 GHz. These correspond to 1σ thermal noise values of 0.08 mJy and 0.013 mJy per $\sim 10 \text{ km/s}$ channel in one hour, at frequencies of 200 MHz ($z_{abs} \sim 6.1$) and 500 MHz

($z_{\text{abs}} \sim 1.8$), respectively.

We will use an HI column density of $2 \times 10^{20} \text{ cm}^{-2}$ (i.e. the “classic” definition of a DLA; [67]) and a high spin temperature of 5000 K to estimate the background flux densities toward which the SKA will be able to detect 21 cm absorption. Of course, colder gas will be detected against weaker sources. Note that, while WNM kinetic temperatures are likely to lie in the range $\sim 5000 - 10000 \text{ K}$ [69], Figure 2 of [39] shows that these correspond to $T_s \lesssim 5000 \text{ K}$, for two-phase media and pressures $P/k \lesssim 6000 \text{ cm}^{-3} \text{ K}$. We hence use $T_s = 5000 \text{ K}$ for the current estimates.

Even at its lowest sensitivity, at 200 MHz, equation (1) shows that 12 hour SKA integrations will be able to detect 21 cm absorption at the 5σ level toward 100 mJy background sources, for the above values of N_{HI} and T_s . At lower absorption redshifts, $z_{\text{abs}} \lesssim 2$, where the SKA has a significantly higher sensitivity, it will detect absorption toward far weaker sources (with flux densities $\sim 20 \text{ mJy}$ in the same integration time), as well as detecting the absorption against the numerous 100 mJy sources in half hour integrations that are suitable for extensive surveys. Note that even deep SKA integrations lasting 360 hours will only detect M_{HI}^* galaxies in 21 cm *emission* out to redshifts $z \sim 2.5$, and $0.1 M_{\text{HI}}^*$ systems out to $z \sim 1$. (Galaxies at the knee of the $z \approx 0$ luminosity function have $M_{\text{HI}}^* = 10^{9.79} M_{\odot}$ for $H_o = 75 \text{ km s}^{-1} \text{ Mpc}^{-1}$ [72].) Clearly, it will be difficult to use 21 cm emission searches to trace galactic evolution, if hierarchical merger models are indeed correct. And, since a high signal-to-noise ratio is needed for kinematic studies, these will only be possible out to $z \sim 1$, even for 360 hour integrations on M_{HI}^* galaxies.

2. Frequency coverage and RFI : The SKA will have frequency coverage from $\sim 100 \text{ MHz}$ to $\sim 25 \text{ GHz}$ and will thus be sensitive to 21 cm absorption out to redshifts $z_{\text{abs}} \lesssim 13$. It is likely to be built on a site with low terrestrial radio background is low, and it will also be one of the first radio telescopes to incorporate modern RFI mitigation techniques (e.g. [11,24]), crucial for observations at these frequencies. These techniques will make it possible for the SKA to reach theoretical noise levels in unprotected radio bands.

3. Survey capabilities : The SKA will have a wide-band correlator with the ability to handle 10^4 channels over a large input bandwidth. In combination with its wide field of view (200 square degrees at 0.7 GHz) large instantaneous bandwidth (2 bands, each with a full width equal to a fourth of the centre frequency of the observing band) and unequaled low frequency coverage, the SKA will be wonderfully suited for blind 21 cm absorption surveys, never before possible with an interferometer.

4. Angular resolution : The SKA will have an angular resolution better than $(0.02/\nu_{\text{GHz}})''$, with excellent U-V coverage. This corresponds to spatial resolutions of $\sim 350 \text{ pc}$ at $z \sim 2$ and $\sim 600 \text{ pc}$ at $z \sim 6$. Remarkably, this is somewhat better than the typical spatial resolution obtained in HI emission studies of the kinematics of local galaxies (e.g. [58]).

8. Blind SKA surveys

The sensitivity of a blind survey for redshifted absorption can be quantified by the total redshift path surveyed and the sensitivity function (i.e. the number of lines of sight at a given redshift with detectable absorption; e.g. [57]). In the case of the SKA, the sensitivity function of a 21 cm absorption survey (out to $z \sim 13$) is determined by the number of radio sources available as background targets at a given redshift, with sufficiently high flux density to show detectable 21 cm absorption. We have seen in Section 7 that twelve hours of SKA integration will be sufficient to detect 21 cm absorption at the 5σ level in all DLAs ($N_{\text{HI}} > 2 \times 10^{20} \text{ cm}^{-2}$ and $T_s < 5000 \text{ K}$) toward 100 mJy sources out to $z \sim 6$ and toward even weaker sources at lower redshifts. We will hence use a flux cut-off of 100 mJy at the redshifted 21 cm frequency to estimate the number of sources available as background targets for a blind survey.

The temporal evolution of the bright end of the radio luminosity function is reasonably well-understood out to $z \sim 4$, based on low frequency radio samples [28,29,62]. We have used the results from [29] to estimate the number of radio galaxies available as absorption targets for the

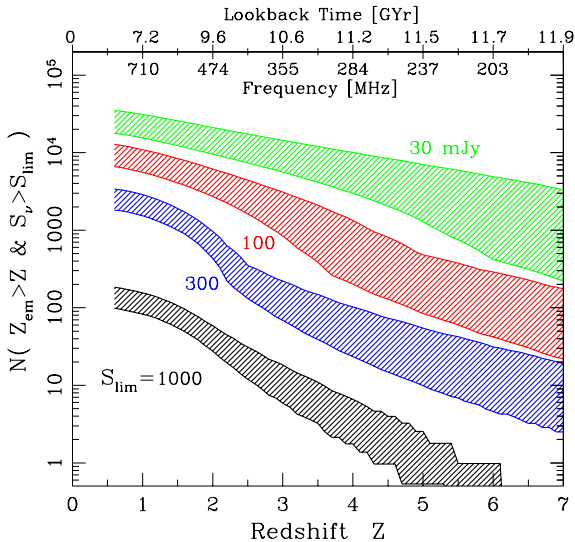


Figure 5. The number of background radio galaxies per 2π steradians with redshift greater than z and flux density greater than S_{lim} at frequency $f = 1420(1+z)^{-1}$ MHz, for $S_{lim} = 30, 100, 300$ and 1000 mJy. The bands indicate the range of uncertainty that spans the no-evolution and mild (1σ) evolution cases [29].

SKA. Note that radio galaxies form ideal background sources, since they have sufficient angular extent to probe galactic scales (one to tens of kpc) in a foreground absorber. Fig 5 shows the number of radio sources above a given flux density that will be available for absorption studies at different redshifts; this has been done for four limiting flux densities, $S_{lim} = 30, 100, 300$ and 1000 mJy, calculated at the redshifted 21 cm line frequency. The bands in the figure indicate the range of uncertainty spanning the no-evolution and mild (1σ) evolution cases described by [29]. We restrict the following discussion to $z \lesssim 4$ to avoid speculative extrapolations in source number counts.

Fig. 5 shows that there should be of order 10^3 radio sources per hemisphere of the sky with $z > 4$, whose flux densities at 284 MHz (corresponding to the HI line at $z = 4$) exceed 100 mJy. The survey sensitivity function at $z \sim 4$ is thus ~ 1000 , a factor of 20 larger than the combined sensitivity of all current optical DLA surveys at this redshift (see Fig. 5 of [57]). The DLA statistic $n_{DLA}(z) = dN/dz$ quantifies the expected number of interceptions of $N_{HI} > 2 \times 10^{20} \text{ cm}^{-2}$ absorbers that will occur per unit redshift. This interception rate rises steadily to the range 0.3 to 0.4 for redshifts greater than 4 [50]. Note that the $z \sim 4$ sources probe absorbing galaxies through 90% of the age of the Universe. Further, a number of 30 mJy sources will show “associated” absorption at these redshifts, which will be stronger due to the higher metallicity and dust content near the nuclei of the radio galaxies and quasars. This will allow the measurement of redshifts of young radio galaxies (regardless of their dusty cocoons), independent of optical spectroscopy.

Of course, the SKA sensitivity is at its lowest below ~ 300 MHz [30]. At ~ 500 MHz (i.e. $z \sim 1.85$, for the HI line), it will be possible to detect 21 cm absorption in DLAs toward 20 mJy sources (see Section 7). The survey sensitivity function at $z \sim 2$ is thus $> 2 \times 10^4$, more than two orders of magnitude larger than the combined value from present optical surveys [57].

Clearly, blind SKA 21 cm absorption surveys will allow the construction of unparalleled samples of “normal” galaxies out to $z \gtrsim 4$. As men-

tioned earlier, these will be unbiased by dust extinction and thus well-suited to study the evolution of typical galaxies with redshift. We note, finally, that observing time requirements are drastically alleviated by the large beam of the SKA (~ 200 square degrees at 0.7 GHz; [30]); this allows spectra of a large number of sources to be taken simultaneously, at any given frequency setting.

In summary, the SKA will be able to carry out 21 cm absorption measurements against thousands of distant radio sources out to redshifts of four or greater, allowing detailed studies of galaxies that intervene by chance along the line of sight. These include the kinematics and dynamical masses of the absorbers, their gaseous extent and the structure of their ISM. In addition, blind 21 cm absorption surveys will give rise to large unbiased samples of gas-rich intervening galaxies, allowing us to determine the size and mass of normal galaxies as a function of redshift and to thus directly test theoretical models of structure formation. These surveys will also provide large samples of associated absorbers, enabling studies of the evolution in the environment of active galactic nuclei from high redshifts to the present epoch.

Acknowledgments We are grateful to Sandhya Rao and Susan Ridgway for kindly providing us with the damped Lyman- α profile toward QSO 0738+313 and a fully processed HST image of 3C196, respectively. NK thanks Jayaram N Chengalur for permission to present unpublished results on 3C196 and PKS 1229–021.

REFERENCES

1. P.D. Barthel, *ApJ* 336 (1989) 606.
2. R.H. Becker et al., *AJ* 122 (2001) 2850.
3. R. Braun and R. Walterbos, *ApJ* 386 (1992) 120.
4. C. de Breuck et al., *A&A* 352 (1999) L51.
5. C. de Breuck et al., *A&A* 401 (2003) 911.
6. W. van Breugel et al., *ApJ* 518 (1999) L61.
7. F.H. Briggs et al., *ApJ* 341 (1989) 650.
8. F.H. Briggs, E. Brinks and A.M. Wolfe, *AJ* 113 (1997) 467.
9. F.H. Briggs, *ASP Conf. Ser.* 156: Highly Redshifted Radio Lines, p. 16, 1999.
10. F.H. Briggs, *Perspectives on Radio Astronomy: Science with Large Antenna Arrays*, p. 75, 2000.
11. F.H. Briggs, J.F. Bell, M.J. Kesteven, *AJ* 102 (2000) 3351.
12. F.H. Briggs, A.G. de Bruyn and R.C. Vermeulen, *A&A* 373 (2001) 113.
13. V. le Brun et al., *A&A* 321 (1997) 733.
14. C.L. Carilli et al., *AJ* 111 (1996) 1830.
15. J.N. Chengalur and N. Kanekar, *MNRAS* 302 (1998) L29.
16. J.N. Chengalur, A.G. de Bruyn and D. Narasimha, *A&A* 343 (1999) L79.
17. J.N. Chengalur and N. Kanekar, *MNRAS* 318 (2000) 303.
18. J.G. Cohen, *AJ* 121 (2001) 1275.
19. J.E. Conway and P.R. Blanco, *ApJ* 449 (1995) L131.
20. S.L. Ellison et al., *A&A* 379 (2001) 393.
21. S.M. Fall and Y.C. Pei, *ApJ* 402 (1993) 479.
22. X. Fan et al., *AJ* 123 (2002) 1247.
23. G.B. Field, *Proc. I. R. E.* 46 (1958) 240.
24. P.A. Fridman and W.A. Baan, *A&A* 378 (2001) 327.
25. M. Fukugita, C.J. Hogan and P. Peebles, *ApJ* 503 (1998) 518.
26. J.H. van Gorkom et al., *AJ* 97 (1989) 708.
27. M.G. Haehnelt, M. Steinmetz and M. Rauch, *ApJ* 495 (1998) 64.
28. M.J. Jarvis and S. Rawlings, *MNRAS* 319 (2000) 121.
29. M.J. Jarvis et al., *MNRAS* 327 (2001) 907.
30. D.L. Jones, *SKA Memo* 45 (2004).
31. N. Kanekar and J.N. Chengalur, *A&A* 369 (2001) 42.
32. N. Kanekar and J.N. Chengalur, *A&A* 399 (2003) 857.
33. N. Kanekar and F.H. Briggs, *A&A* 412 (2003) L29.
34. N. Kanekar et al., in preparation (2004).
35. N. Kanekar and J.N. Chengalur, in preparation (2004).
36. S.R. Kulkarni and C. Heiles, *Galactic and Extra-Galactic Radio Astronomy*, p. 95, 1988.
37. W. Lane et al., *AJ* 116 (1998) 26.
38. W.M. Lane, F.H. Briggs and A. Smette, *ApJ*

- 532 (2000) 146.
39. H. Liszt, *A&A* 371 (2001) 698.
40. P. Madau et al., *MNRAS* 283 (1996) 1388.
41. R. Morganti et al., *MNRAS* 323 (2001) 331.
42. D.B. Nestor, S.M. Rao and D.A. Turnshek, *ASSL Vol. 281: The IGM/Galaxy Connection. The Distribution of Baryons at $z=0$* , p. 27, 2003.
43. P.P. Papadopoulos et al., *ApJ* 528 (2000) 626.
44. Y.C. Pei, M. Fall and M.G. Hauser, *ApJ* 522 (1999) 604.
45. P. Petitjean, R. Srianand and C. Ledoux, *A&A* 364 (2000) L26.
46. M. Pettini et al., *ApJ* 510 (1999) 576.
47. Y.M. Pihlström, J.E. Conway and R.C. Vermeulen, *A&A* 404 (2003) 871.
48. J.X. Prochaska and A.M. Wolfe, *ApJ* 487 (1997) 73.
49. J.X. Prochaska et al., *ApJS* 147 (2003) 227.
50. J.X. Prochaska and S. Herbert-Fort, *PASP* 116 (2004) 622.
51. S. Rao, F.H. Briggs *ApJ* 419 (1993) 515
52. S.M. Rao and D.A. Turnshek, *ApJS* 130 (2000) 1.
53. S.M. Rao et al., *ApJ* 595 (2003) 94.
54. S.E. Ridgway and A. Stockton, *AJ* 114 (1997) 511.
55. M. Schmidt, D.P. Schneider and J.E. Gunn, *AJ* 110 (1995) 68.
56. C.C. Steidel et al., *ApJ* 519 (1999) 1.
57. L.J. Storrie-Lombardi and A.M. Wolfe, *ApJ* 543 (2000) 552.
58. R.A. Swaters et al., *A&A* 390 (2002) 829.
59. A. Taramopoulos, F.H. Briggs, D.A. Turnshek, *AJ* 107 (1994) 1937.
60. R.C. Vermeulen et al., *A&A* 404 (2003) 861.
61. S.D.M. White and C.S. Frenk, *ApJ* 379 (1991) 52.
62. C.J. Willott et al., *MNRAS* 322 (2001) 536.
63. A.M. Wolfe et al., *ApJ* 208 (1976) L47.
64. A.M. Wolfe and M.M. Davis, *AJ* 84 (1979) 699.
65. A.M. Wolfe, F.H. Briggs and D.L. Jauncey, *ApJ* 248 (1981) 460.
66. A.M. Wolfe et al., *ApJ* 294 (1985) L67.
67. A.M. Wolfe et al., *ApJS* 61 (1986) 249.
68. A.M. Wolfe, E. Gawiser and J.X. Prochaska, *ApJ* 593 (2003) 235.
69. M.G. Wolfire et al., *ApJ* 443 (1995) 152.
70. M. Zwaan, M. Verheijen, M., F.H. Briggs, *PASA* 16 (1999) 100
71. M. Zwaan, F.H. Briggs, M. Verheijen, *ASP Conf. Ser. 254: Extragalactic Gas at Low Redshift*, p.169 (2002)
72. M.A. Zwaan et al., *AJ* 125 (2003) 2842.